A. Strom · L. Li · H. Lan

Rock avalanche mobility: optimal characterization and the effects of confinement

Abstract A Central Asia rock avalanche (rockslide) inventory that includes about 600 case studies with measured parameters is used to present a quantitative characterization of rock avalanche mobility and its dependence on the controlling parameters such as volume and height drop. The mobility can be characterized by runout and angle of reach, as well as by the affected area. The database was analyzed after dividing the rock avalanches into three confinement categories—frontally confined, laterally confined, and unconfined. In addition to the traditionally used slope failure volume and height drop, we correlated mobility parameters with their product that is proportional to the potential energy released during rock avalanche emplacement. It was found that coefficients of determination of the regressions of the affected area with volume and, especially, with its product with maximal height drop are higher than those of volume with runout and much higher than those of volume with angle of reach for all confinement conditions. Thus, these relationships provide an optimal characterization of the rock avalanche mobility. Relative influence of failure volume and height drop on rock avalanche mobility was also analyzed. The regression equations obtained in this study were successfully applied to several case studies from other mountain regions. The proposed regression equations can be used to predict the exposure of elements at risk threatened by anticipated rock avalanches. They can also be used to estimate the parameters of rockslide dams that might originate at the sites with anticipated large-scale rock slope failures, if their volumes and height drops can be assessed. The confinement conditions are statistically proved to influence the rock avalanche mobility and must be taken into consideration during hazard and risk assessment.

Keywords Rockslide · Rock avalanche · Mobility · Confinement

Introduction

Rock avalanches produced by large-scale catastrophic bedrock landslides (rockslides) are among the most hazardous natural phenomena endangering people in mountainous regions. Usually, the collocation "rock avalanche" is used to describe long runout features, while rock slope failures that form compact bodies in narrow valleys are called "rockslide." However, if we keep in mind the internal structure and grain-size composition of the deposits and mechanics of their motion, we can conclude that many, if not most, of the large-scale bedrock landslides, both long runout and compact, have been transformed into flow-like granular flows and, thus, can be classified as rock avalanches (Hungr et al. 2014). Only some rock slope failures remain as "slides" up to the halt of their motion, and should be classified as rockslides. The Central Asian bedrock landslide database (Strom and Abdrakhmatov 2018) analyzed in this study includes both rockslides and rock avalanches that were analyzed simultaneously. Hereafter, we use both terms—"rockslide" and "rock avalanche"—considering that rock avalanches always initiate as rockslides.

The extreme mobility of rock avalanches is governed not by the presence of the significant amount of water mixed with debris as in debris flows, but by the processes evolving during emplacement within moving rockslide body and at its base. Various mechanical models were proposed to explain so high mobility of rock avalanches (e.g., Hsü 1975; Grigorian 1979; Davies 1982; Melosh 1986; Kobayashi 1997; Denlinger and Iverson 2001; Iverson and Denlinger 2001; Pollet et al. 2005; Dubovskoi et al. 2008; Strom and Pernik 2013), and the dynamic fragmentation model seems to be the most realistic and well-grounded one (e.g., Davies et al. 2017).

Rock avalanches move at a very high speed—often more than 100 km/h, sometimes affecting vast areas at the base of mountain ranges up to 100 km² and even more (e.g., Reznichenko et al. 2017), and spreading for up to tens of kilometers from the slope base (e.g., Crosta et al. 2015). Their mobility is characterized by the geometrical parameters—runout, angle of reach, and affected area. Actual measurements of rock avalanche velocity are quite rare (see, e.g., Adushkin 2006) and this parameter, intimately connected with mobility, can be hardly analyzed statistically.

Optimal characterization of rock avalanche mobility, besides its scientific merit, is critically important to quantify hazard provided by future large-scale rock slope failures that are inevitable in mountainous regions, and to assess associated risks. As it was pointed out in Iverson (2006) such assessment can be done in two basic ways—by the numerical modeling (Sassa et al. 1994, 2010; Hungr 1995; Denlinger and Iverson 2001; Crosta et al. 2003; McDougall and Hungr 2004; Iverson 2006; Hungr and McDougall 2009), or by use of the empirical relationships between parameters of rock avalanches' (rockslides') source zones and the geometrical parameters that can characterize the affected zones, in other words—the exposure (Corominas et al. 2014, 2015). Numerical modeling is rather laborious, as it requires detailed data on the topography and mechanical properties of rocks affected by slope failure. Besides, it requires knowledge of physics of rock avalanche motion that is still not fully understood. Use of the empirical relationships, especially of those with high coefficients of determination (R^2), allows simple and sufficiently accurate prediction of the runout distance and affected area. Such relationships can also provide some information that could be useful for better understanding of the nature of rock avalanches' extreme mobility.

The most commonly used parameters characterizing mobility are the runout—maximal horizontal distance between headscarp crown and most distant point of the deposits (Kilburn and Sørensen 1998; Legros 2002), and the angle of reach or "fahrborshung"—a term introduced by A. Heim (1932)—ratio between height drop and runout (Sheidegger 1973; Hsü 1975; Davies 1982; Li 1983; Shaller 1991; Nicoletti and Sorriso-Valvo 1991; Kobayashi 1993, 1997; Corominas 1996). Starting from Heim (1932), Sheidegger (1973), and Abele (1974), researchers had analyzed dependence of these parameters on the slope failure volume.

It seems, however, that these unidimensional (runout) or dimensionless (angle of reach) parameters are not the only, and likely not the optimal variables to characterize rock avalanche mobility, especially for the purpose of risk assessment that requires knowledge of the exposure of elements at risk (Corominas et al. 2014, 2015). Indeed, rock avalanche debris can move not only forward, but also laterally, forming fan-shaped or isometric bodies that, although they might travel not as far as those moving straight forward, could affect a much larger area, thus increasing the exposure. Dependence of the deposits' area on slope failure volume was analyzed by Li (1983), Hungr (2006), Legros (2006), and by Griswold and Iverson (2008). All these studies were based on rather limited, less than ca. 200, number of events included in the databases.

It is also obvious that shape of rock avalanche deposits and their geometrical parameters such as runout and area strongly depend on the morphology of the transition and deposition zones and, first of all, on the confinement affecting debris spreading. Following Shaller (1991), all rock avalanches can be divided, at first approximation, into three main groups—unconfined (Fig. 1), laterally confined (channelized) (Fig. 2), and frontally confined (Fig. 3). Similar division, though using different terms, was
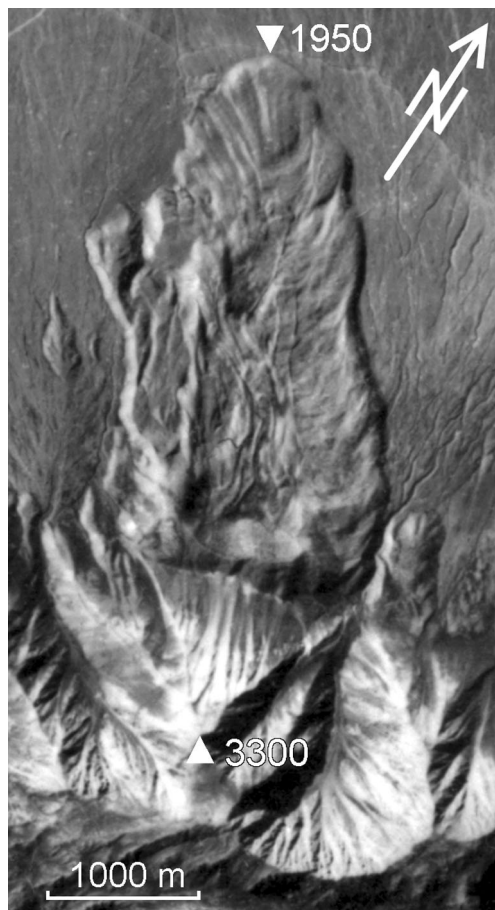

Fig. 2 The laterally confined 6.48-km-long Karakystiak rock avalanche (42.58° N, 73.13° E Northern Tien Shan, Kazakhstan) with funnel-shape headscarp up to 1.95-km wide (between elevation marks 3500 and 3470 m a.s.l.) and distinct trimlines along the initial part of its transition zone (marked at 2780 m and 2930 m a.s.l.) up to 200 m above the resultant surface of the deposits. After Strom and Abdrakhmatov (2018) with permission from Elsevier

proposed by Nicoletti and Sorriso-Valvo (1991). The effects of different confinement conditions were also analyzed by Corominas (1996). Physical significance of confinement can be illustrated by Fig. 4 presenting simplified 2D models of the unconfined and laterally confined rock avalanches (1 on Fig. 4) and of the frontally confined rock avalanche (2 on Fig. 4). While the processes governing debris motion up to point "A" are the same for all three confinement types, after passing this point, they differ. In case 1, further motion depends on basal friction and on internal processes in moving debris (fragmentation, internal friction, heating, etc.). In case 2, in addition to all abovementioned, moving debris has to overcome gravity force and, also, some energy could be consumed by direct collision (impact) with an obstacle. Physical differences between the laterally confined and unconfined cases are predetermined by the potential ability of the latter's to spread laterally (though this ability is not materialized in all cases).

However, most of the empirical relationships mentioned above were derived for the entire data sets without differentiating of the confinement types. The rare exceptions are the abovementioned publications of Shaller (1991) based on 182 case studies and of
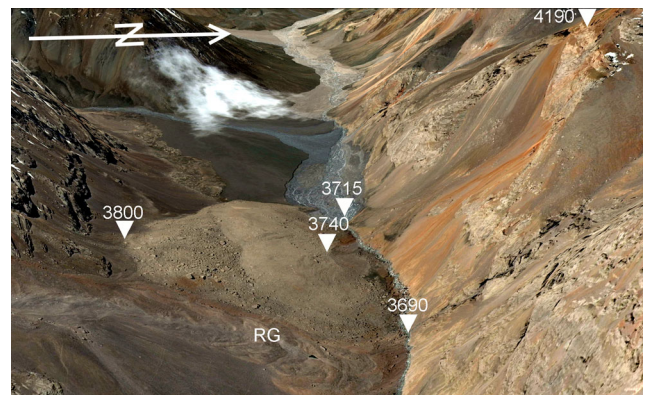

Fig. 1 The unconfined Chaartash-3 rock avalanche (41.25° N, 74.0° E, Central Tien Shan, Kyrgyzstan). Debris moved straight forward without lateral spreading. A fragment of the KFA-1000 satellite image. Here and hereafter, numbers are elevations in meters above sea level of points marked by triangles

Fig. 3 The frontally confined rockslide (rock avalanche) in the Kainar River valley (41.41° N, 77.90° E, southern part of Central Tien Shan, Kyrgyzstan). RG – rock glacier from the tributary valley. 3D Google Earth view. After Strom and Abdrakhmatov (2018) with permission from Elsevier
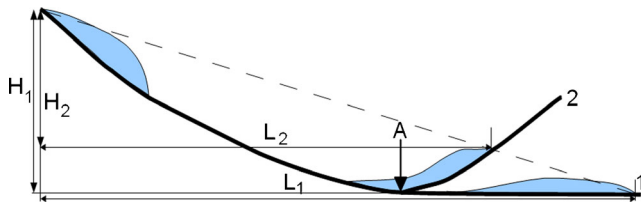
Fig. 4 General 2D models of the unconfined and the laterally confined rock avalanches (1) and of the frontally confined rock avalanches (2). Despite significant difference between H_1 and H_2 and between L_1 and L_2, H/L ratio (angle of reach) for both cases is the same. Point "A" marks the limit beyond which forces governing rock avalanche motion differ. Modified from Strom and Abdrakhmatov (2018) with permission from Elsevier

Nicoletti and Sorriso-Valvo (1991) who analyzed 41 case studies. Corominas (1996) analyzed a large database of 2004 case studies, considering confinement, but his database included landslides of different types, not only rock avalanches. Much larger Central Asian rock avalanche (rockslide) database that includes nearly 1000 case studies, about 600 of which have been quantified (Strom and Abdrakhmatov 2018; Strom 2018) allowed more statistically representative analysis of the relationships between various parameters and selection of optimal parameters characterizing rock avalanches' mobility with due regard to the three basic confinement types.

Rock avalanche database

Study region and database completeness

Database discussed in this paper includes rock avalanches from the Pamir, the Tien Shan, and the Dzungaria mountain systems located in Afghanistan, China, Kazakhstan, Kyrgyzstan, Tajikistan, and Uzbekistan (Fig. 5). The Central Asia region is really one of the global landslide "hotspots" (Nadim et al. 2006) with numerous rockslides and rock avalanches, most of which are prehistoric (Strom and Abdrakhmatov 2018). Mountain ranges are composed of various types of sedimentary, igneous, volcanic and metamorphic rocks of ages ranging from the Precambrian to the Neogene. Rockslides and rock avalanches included in the database can be

ascribed to almost all known types of bedrock landslides included in the latest classification system (Hungr et al. 2014). We have to point out once more that all features classified as "rock avalanche" had originated as slides of various types and, more rarely, as topples, and had been transformed into flow-like rock avalanches during their motion. Taking this into account, along with the fact that local structure and actual mechanical properties (bulk density, compression and tension strength, etc.) of various types of rocks at the particular sites are unknown, we divided the entire database into three groups according to the confinement types only and ignored the initial slope failure mechanism and rock types in the source zones.

Quantitative parameters (volume, height drop, runout, affected area) that will be listed and described in the next section have been measured up to now for about 60% of the case studies identified. For eastern (Chinese) and northeastern (Kazakh) parts of the study region, percentages of the quantified case studies are higher and reach 90%. However, the comparative analysis of size (volume)—frequency distributions for the entire Central Asia region (595 cases), for its Chinese and Kazakh parts (251 cases) and for the remaining parts of the region (344 cases) showed that results of the statistical analysis of the incomplete general database can be considered to be representative (Strom 2018).

Slope failure and resultant rock avalanche parameters and their measurement accuracy

Each case study included in the database and quantified is characterized by numerous parameters such as height of the headscarp or of the source slope (H_s), height drop (maximal—H_{max}, and to the deposits tip—H), volume of failure (V), runout (L), area of the deposits (A_{dep}), total affected area (A_{total}), etc. Their detailed description and principles of measurement are described in Strom and Abdrakhmatov (2018) Chapter 6. Here, we will focus just on some of these parameters that will be analyzed for pair and triple correlations between parameters characterizing rock avalanche mobility (runout, area, their inverse ratios with height drop) and those characterizing slope failure (volume, height drop). Most of these parameters were derived from the analysis of landslides identified on high-resolution satellite images whose

Fig. 5 A, the 30" SRTM DEM of the study region (Dzungarian Range – DJU, Tien Shan and Pamir); B, location of the study region (outlined) in Asia; AFG Afghanistan, CHI China, KAZ Kazakhstan, KYR Kyrgyzstan, TAJ Tajikistan, UZ Uzbekistan

digitized contours were overlaid on the 3" SRTM DEM (digital elevation model provided by the Shuttle Radar Topography Mission in 2000).

Headscarp height or the source slope height (H_s) is measured as the elevation difference between the headscarp crown and the base of the collapsed slope marked by point "A" on Fig. 4. While the crown elevation can be determined easily, the precise localization of the slope base is not so unequivocal. Sometimes it can be defined clearly, but in many cases, it is hidden under the proximal debris accumulation, often of the unknown thickness. In such cases, the headscarp height can be determined with an uncertainty of ± 10 to 15%.

Maximal height drop (H_{max}) is defined as the elevation difference between the headscarp crown and the lowermost point of the deposits. For the cases, where rockslide body had moved downslope gradually and practically did not escape from the headscarp, it is equal to the headscarp height H_s (such slope failures cannot be classified as rock avalanches, but were included in the database). For the frontally confined rock avalanches, it is measured as the elevation difference between the headscarp crown and the lowermost point of the dam's base at its axial line (H_1 for case 2 on Fig. 4). For the laterally confined and unconfined cases, this parameter is the same as elevation difference between the headscarp crown and the lowermost tip of the deposits (H). Accuracy of its measurement is high for the laterally confined and unconfined cases where both points (crown and tip) can be defined directly and depends on how detailed the map is, or on the resolution of the DEM. For the frontally confined cases, accuracy seems to be lower and depends on the steadiness of the pre-slide stream thalweg profile.

Height drop to the tip (H) is the same as H_{max} for the laterally confined and unconfined rock avalanches and can be significantly less for the frontally confined features (case 2 on Fig. 4). In most of cases, its accuracy is high, except rare cases where frontal part of the deposits, including their distal edge, was eroded completely.

Failure volume (V) estimates presented in the database (Strom and Abdrakhmatov 2018) have been assessed case by case as

volume of rock avalanche (rockslide) deposits. Sometimes the headscarp volume was measured to check the reliability of the previous estimates. Possible errors are caused by drastic irregularities of both the headscarp and the deposits shape, lack of data on the pre-failure topography, significant reshaping of the deposits by erosion, and unknown extents of the material entrainment and of rockslide debris softening during its emplacement. Even for the historical rockslides, where the pre-slide topography is known, volumes have been often estimated with quite large scatter. Due to all the above uncertainties, we estimate general accuracy of volume measurements presented in the database as up to ± 50%. However, since volume of all features included in the database differ by more than four orders of magnitude (from less than 1 million cubic meters to ca. 10 km³), such accuracy can be considered to be acceptable.

Runout (L) was measured as the horizontal distance from the headscarp crown to the deposits' tip along the approximate central line of the deposits. This path might be straight, broken, or curved. Accuracy of this parameter assessment is considered to be high; possible errors caused by the erosion of the distal part of the deposits and the irregularity of the travel path when the central line can be traced in different ways, should not exceed ca. 10%.

Area of the deposits (A_{dep}) is one of the most precisely measured parameters whose accuracy depends on the correctness of the rockslide deposits identification and digitization. It is measured in plan view. Possible errors are caused by masking of the deposits by dammed lake water or by lake sediments and by their partial erosion. During the compilation of the database, Strom and Abdrakhmatov (2018) strove to map the area initially covered by rockslide debris. Sometimes, however, more than 50% of the area originally covered by rockslide debris has been eroded (Fig. 6b), same as in other parts of the world (e.g., Hewitt 1998). In such cases, the accuracy of area measurement might decrease significantly.

Total affected area (A_{total}) is the horizontal projection of the polygon that includes the headscarp, the transition zone along which moving debris had passed, and the depositional area. This
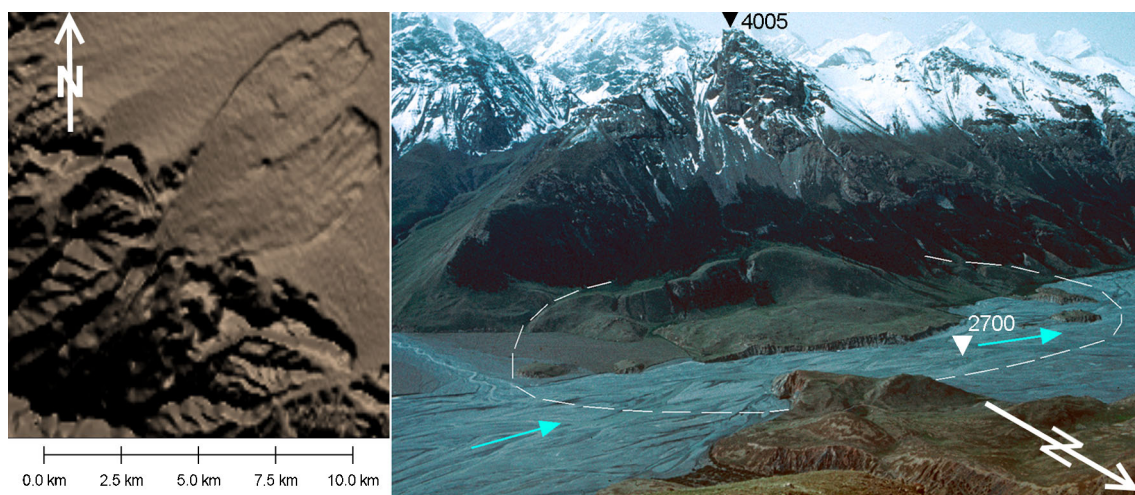

Fig. 6 Left, the fan-shape Yimake rock avalanche (39.2° N, 75.15° E, Eastern Pamir, China. 3" SRTM DEM visualized by Global Mapper software); right, the Atdjalau rock avalanche with strongly eroded isometric body (42.15° N, 79.46° E, Tien Shan, Kyrgyzstan); dashed line marks its approximate initial boundary; blue arrows indicate river flow direction

Table 1 Coefficients of the log-log (power) regressions between various parameters characterizing rock avalanches

Confinement	$L = f(V)$ $\log(L) = a + b \times \log(V)$ $L = 10^a \times V^b$			$H/L = f(V)$[#] $\log(H/L) = a + b \times \log(V)$ $H/L = 10^a \times V^b$			$L = f(V \times H_{max})$ $\log(L) = a + b \times \log(V \times H_{max})$ $L = 10^a \times (V \times H_{max})^b$		
	R^2[*]	$a\ (SE_a)$[**]	$b\ (SE_b)$[***]	R^2[*]	$a\ (SE_a)$[**]	$b\ (SE_b)$[***]	R^2[*]	$a\ (SE_a)$[**]	$b\ (SE_b)$[***]
Frontally confined	0.7335	−0.1057 (0.0136)	0.2619 (0.0091)	0.3008	−0.3529 (0.0131)	−0.0984 (0.0089)	0.8160	0.6635 (0.0142)	0.2282 (0.0063)
Laterally confined	0.7301	0.0279 (0.0247)	0.3024 (0.0159)	0.4497	−0.3690 (0.0168)	−0.1127 (0.0109)	0.0510	0.5246 (0.0860)	0.0709 (0.0377)
Unconfined	0.8066	−0.1729 (0.0228)	0.3492 (0.0196)	0.3962	−0.3310 (0.0212)	−0.1232 (0.0179)	0.8824	0.8351 (0.0362)	0.2885 (0.0124)
All	0.7126	−0.0953 (0.0117)	0.2929 (0.0080)	0.3524	−0.3551 (0.0090)	−0.1042 (0.0062)			

Confinement	$A_{total} = f(V)$ $\log(A_{total}) = a + b \times \log(V)$ $A_{total} = 10^a \times V^b$			$H/A_{total} = f(V)$ $\log(H/A_{total}) = a + b \times \log(V)$ $H/A_{total} = 10^a \times V^b$			$A_{total} = f(V \times H_{max})$ $\log(A_{total}) = a + b \times \log(V \times H_{max})$ $A_{total} = 10^a \times (V \times H_{max})^b$		
	R^2[*]	$a\ (SE_a)$[**]	$b\ (SE_b)$[***]	R^2[*]	$a\ (SE_a)$[**]	$b\ (SE_b)$[***]	R^2[*]	$a\ (SE_a)$[**]	$b\ (SE_b)$[***]
Frontally confined	0.9008	−0.6794 (0.0159)	0.5797 (0.0105)	0.8006	0.2569 (0.0158)	−0.3829 (0.0105)	0.9258	0.9791 (0.0168)	0.4849 (0.0076)
Laterally confined	0.8833	−0.7388 (0.0376)	0.6522 (0.0247)	0.8686	0.3932 (0.0270)	−0.4480 (0.0184)	0.9267	1.0884 (0.0357)	0.5497 (0.0163)
Unconfined	0.9151	−0.7312 (0.0286)	0.6981 (0.0242)	0.8330	0.2348 (0.0301)	−0.4701 (0.0245)	0.9361	1.2537 (0.0497)	0.5668 (0.0172)
All	0.8972	−0.7049 (0.0135)	0.6107 (0.0092)						

Confinement	$A_{dep} = f(V \times H_{max})$ $\log(A_{dep}) = a + b \times \log(V \times H_{max})$ $A_{dep} = 10^a \times (V \times H_{max})^b$		
	R^2[*]	$a\ (SE_a)$[**]	$b\ (SE_b)$[***]
Frontally confined	0.9064	0.7954 (0.0197)	0.5039 (0.0089)
Laterally confined	0.9150	0.9748 (0.0394)	0.5745 (0.0182)
Unconfined	0.9111	1.1283 (0.0607)	0.5769 (0.0210)

[*] R^2: coefficients of determination of the log-log regressions (power regressions)

[**] $a\ (SE_a)$: estimated coefficients a of the log-log regressions and the corresponding standard errors (SE)

[***] $b\ (SE_b)$: estimated coefficients b of the log-log regressions and the corresponding standard errors (SE)

[#] H/L vs. V relationships were plotted in Fig. 7b in semi-log form

parameter is important for hazard assessment as it describes the entire area directly affected by rock avalanche (rockslide). Besides, this parameter is better associated with runout then the deposits area, since L can be considered as a unidimensional characteristic (axial line) just of the total affected area. Factors affecting the accuracy of the estimate of this parameter are the same as those for A_{dep}. We should mention that in cases, where the distinct trimlines are visible, outer boundaries of the transition zone were delineated just along such trimlines that could remain much above the resultant deposits' level (Fig. 2).

Failure volume (V) along with parameters describing elevation difference between headscarp crown and deposits base (H_s, H_{max}) characterize the slope failure. Runout (L), angle of reach (H/L), and area, both of the deposits (A_{dep}), and total affected (A_{total}) characterize the result of rock avalanche emplacement.

From the physical point of view, it seems reasonable to measure and analyze vertical descent and horizontal displacement of the center of gravity. Nevertheless, we exclude these parameters due to two main reasons. First, the locations of the initial and final centers of gravity are much more uncertain than those of the headscarp crown and those of the deposits front (tip) or base. Position of the centers of gravity can only be determined more or less precisely for case studies with well-known topographies before and after the event (e.g., Adushkin 2006) and even for such cases, considering topographic irregularities, such assessment is quite laborious. Second, the horizontal distance between the pre- and post-failure center of gravity cannot reflect the real runout (position of the rock avalanche front) and, thus, could not be used to characterize the exposure that is critically important for rock avalanche hazard assessment.

Optimal characterization of mobility: runout versus affected area

As mentioned, most of researchers used H/L ratio ("angle of reach" or "fahrborshung") to characterize rock avalanche mobility and analyzed its correlation with volume of failure, although Legros (2002) pointed out that this ratio has no physical
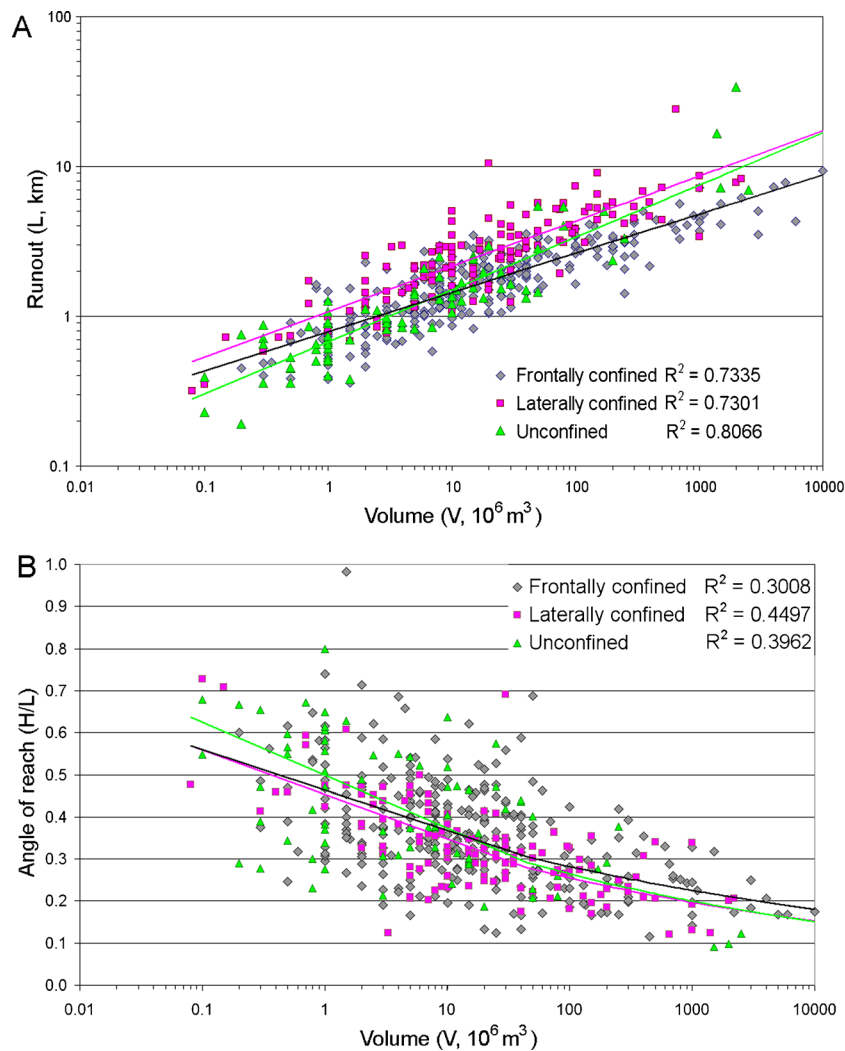

Fig. 7 Relationships between volume (V) of rock avalanches (rockslides) with different confinements and: A, runout (L); B, height drop to runout ratio (H/L). Here and hereafter, corresponding R^2 (coefficient of determination) values of log-log regressions (power regressions) are added to the legend. Modified from Strom and Abdrakhmatov (2018) with permission from Elsevier
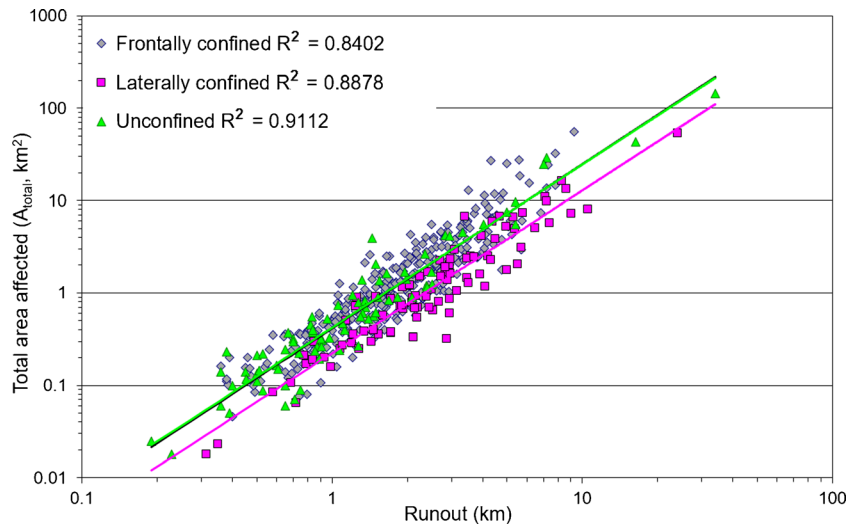
Fig. 8 Relationships and corresponding R^2 values of log-log regressions between total affected area (A_{total}) and runout (L) for rock avalanches (rockslides) with different confinement. After Strom and Abdrakhmatov (2018) with permission from Elsevier

meaning. The more rarely used correlation of runout (L) with volume was investigated. We must note that different authors that analyzed different databases sometimes came to somehow controversial conclusions. For example, Shaller (1991) found that channeling (lateral confinement) and division of the debris into several separate lobes had no significant effects on the mobility characterized by the H/L ratio. An opposite conclusion was made by Nicoletti and Sorriso-Valvo (1991) who found that channeling of debris supported longer runout (L), thus, increasing mobility. Leaping ahead, our results are in line with the latter conclusion.

It seems however, that both L and H/L, does not appear to be the optimal parameter to characterize rock avalanche mobility neither for better understanding of its mechanism(s), nor for risk assessment. The latter requires knowledge of the exposure of elements at risk (Corominas et al. 2014, 2015). However, in the unconfined and frontally confined conditions, rock avalanche debris can move not only straight forward but also laterally. It is most variable for the unconfined cases: some rock avalanche deposits form elongated tongues whose maximal width is almost the same as the headscarp base width (see Fig. 1), while some fan-shape or isometric bodies (Fig. 6) demonstrate significant lateral spreading.

Considering relatively large number of cases included in the Central Asian rock avalanche (rockslide) database (Strom and Abdrakhmatov 2018), we can draw conclusions on which parameter(s) reflect the real dependence between source and resultant rock avalanche' characteristics better by comparing the

coefficients of determination (R^2) of the corresponding regressions listed in Table 1. As mentioned in the "Introduction" section, we analyzed not only runout and angle of reach, but also area—the two-dimensional characteristics of the mobility and their dependence on the parameters characterizing slope failure source.

Unidimensional and dimensionless parameters—runout and angle of reach

It is well known that both runout and angle of reach strongly depend on rock avalanche volume—slope failures with larger volumes produce rock avalanches with larger runout and smaller H/L ratio (Sheidegger 1973; Hsü 1975; Davies 1982; Li 1983; Shaller 1991; Nicoletti and Sorriso-Valvo 1991; Kobayashi 1993, 1997; Corominas 1996; Kilburn and Sørensen 1998; Legros 2002).

Analysis of such relationships for Central Asian case studies revealed a much better correlation between V and L (Fig. 7a) than between V and H/L (Fig. 7b), regardless of the confinement type (Strom and Abdrakhmatov 2018; Strom 2018) (Table 1). Thus, runout seems to be preferable to characterize rock avalanche mobility and can be predicted for a given volume of failure with much higher confidence.

The predicted runout for a given volume differs for different confinement types (Fig. 7a), though corresponding R^2 values are just slightly higher than the R^2 for the entire database (Table 1). This conclusion is highly practical when considering its

Table 2 Relative importance of volume (V) and runout (L) for total affected area (A_{total})

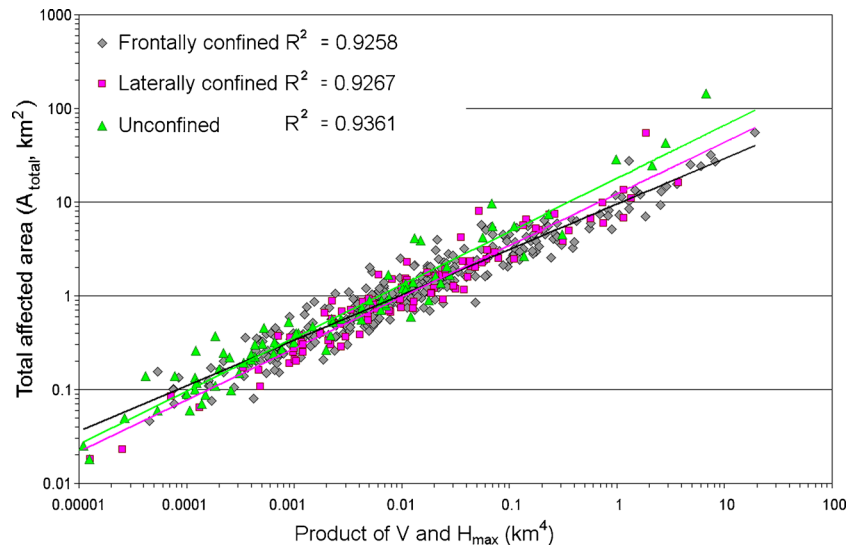| Confinement	Number of cases	Coefficient			R-squared	Relative importance	
		a	b	c		V	L
Frontally confined	294	0.34	0.91	1.47	0.95	0.51	0.49
Laterally confined	68	0.34	0.99	0.49	0.97	0.49	0.51
Unconfined	71	0.38	0.90	1.00	0.96	0.50	0.50

Fig. 9 Relationships and corresponding R^2 values of log-log regressions between total affected area (A_{total}) and product of rockslide volume and maximal height drop ($V \times H_{max}$) for rock avalanches (rockslides) with different confinement. After Strom and Abdrakhmatov (2018) with permission from Elsevier

applicability to predict the distance from the slope foot that might be affected by rock avalanche. Figure 7a shows that the laterally confined rock avalanches have up to ca. two times larger runouts than the frontally confined cases, which is obvious, considering confinement conditions. Behavior of the unconfined rock avalanches is more complex—small-size features are characterized by minimal mean runouts. It can be hypothesized that debris of the unconfined rock avalanches produced by slope failures less than ca. 5×10^6 m³ in volume in most cases spreads both forward and laterally and, thus, there is just not enough material to move for a longer distance from the slope foot. Runouts of largest events, on the contrary, are comparable with those of the laterally confined features of the same volume. This conclusion, however, has a high degree of uncertainty, since number of giant rock

avalanches with such confinement conditions is small and one or few additional very large case studies of these confinement types could change the b value of the corresponding regression equations significantly.

Besides V vs. L correlations, we analyzed relationships between the runout and the product of rock avalanche (rockslide) volume and maximal height drop (parameter, somehow proportional to the potential energy available) that will be discussed hereafter in the "Dependence of the mobility on the potential energy" section.

Two-dimensional parameters—total affected area and area of the deposits
Considering the needs of landslide risk assessment, Strom and Abdrakhmatov (2018) analyzed the dependence of total affected
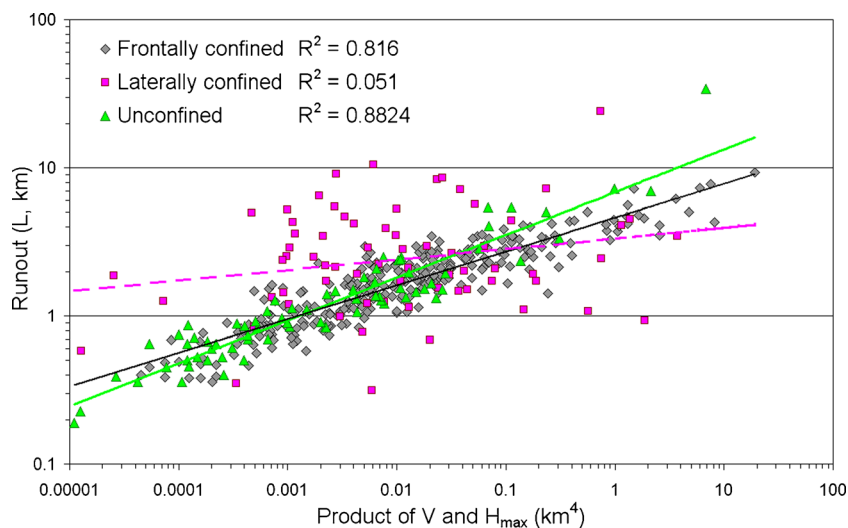

Fig. 10 Relationships and corresponding R^2 values of log-log regressions between runout (L) and product of rockslide volume and maximal height drop ($V \times H_{max}$) for rock avalanches (rockslides) with different confinement. After Strom and Abdrakhmatov (2018) with permission from Elsevier

Fig. 11 Relationships and corresponding R^2 values of log-log regressions between runout (L) and maximal height drop (H_{max}) for rock avalanches (rockslides) with different confinement. After Strom and Abdrakhmatov (2018) with permission from Elsevier
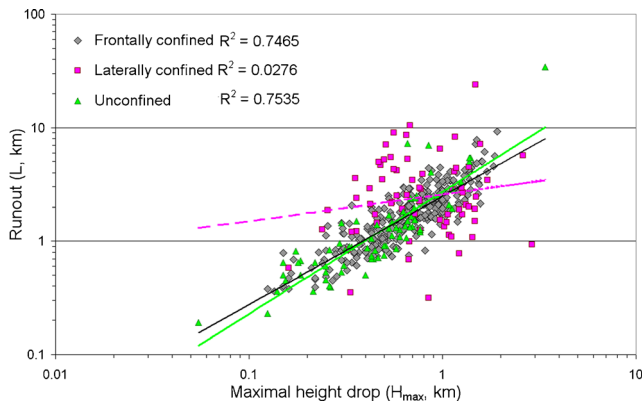
area (A_{total}) on source parameters. Indeed, there is no big difference for an element at risk if the ground would suddenly subside, or if it would be swept away by rapidly moving debris or buried by the deposits—it would be destroyed in all cases. As it was shown by the statistical analysis (Table 1), coefficients of determination for the regressions between rock failure volume and the total affected area (V vs. A_{total}) and for its inverse ratio with height drop (H/A_{total} vs. V) are higher than for those between volume and runout (L vs. V) and between volume and angle of reach (H/L vs. V). While for A_{total} vs. V regressions R^2 values are just slightly (12–19%) larger than those for L vs. V regressions, such values for the H/A_{total} vs. V regressions increase for about two times compared with H/L vs. V regressions. It supports the assumption that affected area reflects rock avalanche mobility much better than just a runout. Similarly to the unidimensional parameter (L), we analyzed the dependence of the two-dimensional parameters (A_{total} and A_{dep}) on the product of rock failure volume and maximal

height drop (H_{max}) too; its results will be described in the next section.

Interesting and somehow surprising results were obtained when we analyzed relationships between runout and total affected area. A_{total} vs. L regression curves for the unconfined and frontally confined cases appeared to be almost the same, while for the laterally confined cases such curve lies parallel but their affected areas are about two times less for the given runout values (Fig. 8). A_{total} vs. L regressions can be described by the power equations in the form: $A_{total} = a \times L^b$. While coefficients "b" for all three confinement types are almost equal (vary from 1.7594 ± 0.0659 to 1.7765 ± 0.0422), coefficient "a" for the frontally confined cases is 0.4134 ± 0.0148, for the unconfined cases is nearly the same (0.4222 ± 0.0248), but for the laterally confined cases is 0.2238 ± 0.0178 only. Similarity of regressions for the unconfined and frontally confined cases allows assumption that lateral spreading due to collision with an opposite slope provides nearly the same effect as lateral spreading of debris moving over an unconfined surface. We must consider, however, that another parameter indirectly affecting these relationships is rock avalanche volume. As it can be seen in Table 2, relative importance of volume and runout for the total affected area derived from the triple regression $\log(A_{total}) = a \times \log(V) + b \times \log(L) + c$ is almost identical ($\pm 1\%$).

Dependence of the mobility on the potential energy

The authors did not find previous publications where the dependence of runout or affected area on the $V \times H$ product was analyzed, despite this parameter being the physically most reasonable since it is proportional at a first approximation to the potential energy released during rockslide motion (E_{pot}). The only exception is the paper of Howard (1973) who presented the relationship between the potential energy and L/H ratio based on 22 terrestrial and 3 lunar case studies. His analysis, however, ignored the fact that correlated variables are not independent—both include H. More strict definition of the potential energy requires knowledge of the height drop of the center of gravity of a displaced rock mass (H_{cg}) and of a rocks' unit weight (ρ): $E_{pot} = V \times \rho \times g \times H_{cg}$, where
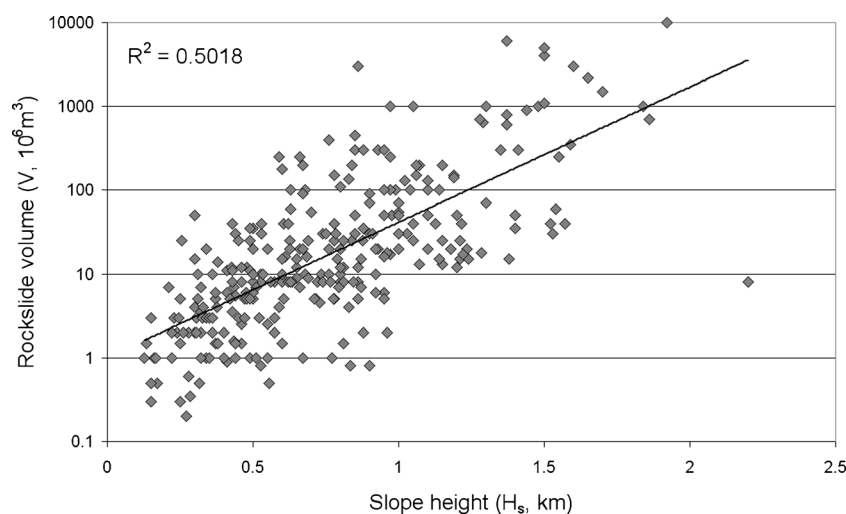

Fig. 12 Relationship between slope height (H_s) and volume (V) for Central Asian rock avalanches (rockslides) that occurred in the frontally confined conditions. Modified from Strom and Abdrakhmatov (2018) with permission from Elsevier

Table 3 Relative importance of volume (V) and maximal height drop (H_{max}) for runout (L)

Confinement	Number of cases	Coefficient a	b	c	R-squared	Relative importance V	H_{max}
Frontally confined	294	0.15	0.57	1.20	0.87	0.49	0.51
Laterally confined	68	0.14	0.94	− 0.65	0.90	0.43	0.57
Unconfined	71	0.22	0.56	0.25	0.91	0.53	0.47

g the is gravitational acceleration. However, considering the headscarp shapes of the majority of rockslides, it can be taken that descent of the center of gravity is about ½ to 1/3 of H_{max}; bulk densities of the most widely distributed rock types differ from ca. 2000 to ca. 3000 kg/m^3, and ranges of estimates of both parameters are comparable with the mean accuracy of volume estimates (about ± 50%) or even less. Meanwhile, volumes of slope failures included in the database vary within more than four orders of magnitude (from ca. 5×10^5 m^3 to ca. 10^{10} m^3). Therefore, influence of the uncertainties of rock density and of the positions of the center of gravity relative to the headscarp crown on the assessment of the potential energy within the entire database is much less than influence of rockslide volumes uncertainty and can be considered to be negligible. Thus, the use of the $V \times H_{max}$ parameter seems to be quite reasonable.

An analysis performed in Strom and Abdrakhmatov (2018) demonstrated that relationships between total affected area (A_{total}) and the product of rock avalanche (rockslide) volume and maximal height drop ($V \times H_{max}$) have the highest coefficients of determination (Fig. 9 and Table 1). Correlations between $V \times H_{max}$ and runout (L) for the unconfined and frontally confined rock avalanches are also characterized by R^2 values that are much higher than those of just V vs. L relationships. However, they are surprisingly low for the laterally confined sampling (Fig. 10 and Table 1), while the A_{total} vs. $V \times H_{max}$ relationship for the same sampling is, practically, almost the same as those for samplings with the other two confinement types (Fig. 9 and Table 1). We also analyzed the relationships between area of the deposits (A_{dep}) and $V \times H_{max}$ and found that they also have coefficients of determination exceeding 0.9, though slightly lower than those for the A_{total} vs. $V \times H_{max}$ relationships (Table 1).

The anomalously low L vs. H_{max} correlation for the laterally confined sampling is caused by lack of correlation between the runout and height drop for this sampling (Fig. 11), while the L vs. V relationship between the runout and volume for the same sample is rather regular (Fig. 7 and Table 1). We must notice, however, that such parameters as volume and height drop are not completely independent. Generally, the higher the slope is, the larger (more voluminous) slope failure might occur on it (Fig. 12). It can be described by the exponential regression: $V = 1.0089 \times e^{0.0037 H_s}$,

however, with large scatter ($R^2 = 0.5018$). Slope height (H_s) plotted on Fig. 12 corresponds to elevation difference from the headscarp crown up to point "A" on Fig. 4 and is equal to H_{max} for the frontally confined rock avalanches for which this relationship was derived. For such confinement conditions, effect of the down-valley debris spreading should be minimal (unlike to lateral confinement) and can be neglected.

Analysis of the relative importance of the input parameters for L vs. $V \times H_{max}$ and A_{total} vs. $V \times H_{max}$ triple correlations shows that H_{max} has larger effect on runout than on area (compare Tables 3 and 4). It explains lack of correlation between runout (L) and $V \times H_{max}$ for rock avalanches that moved in the laterally confined conditions while for other types of confinement coefficients of determination are quite high (see Table 1). In contrast, failure volume provides the main control on the affected area for all confinement types and on runout for the unconfined rock avalanches.

It can be hypothesized that an irregular behavior of many of the laterally confined rock avalanches might be caused by the complexity of their geometries and motion. Indeed, some laterally confined rock avalanches that moved down-valley finally collided with valley slope bend forming thick accumulation with rather small deposits area as it happened with the Seit rock avalanche (Fig. 13). Some other laterally confined cases, on the contrary, turned and continued moving, thus increasing both runout and affected area (Fig. 2). Some laterally confined rock avalanches entered wider valley where debris formed fan-shape bodies, as it occurred at the 1949 Khait rock avalanche (Fig. 14 and also refer to Evans et al. 2009 for more details). Statistical analysis of such complex cases needs much larger database than available now.

In order to understand various factors affecting mobility and of their determination accuracy, one should consider variability of each parameter that can be characterized by the ratio of maximal and minimal parameter values for case studies included in the database (Table 5). From this table, we can see that parameters related to height drop (H_s, H_{max}, H) vary up to ca. 70 times (less than two orders of magnitude), while rockslide volumes vary up to five orders of magnitude. Range of volume variation is approximately equal to a third power of height drop variation (H_s and H_{max}). The latter reflects a linear dimension of the rockslide source and it is quite logical that volume varies proportionally to its third power.

Table 4 Relative importance of volume (V) and maximal height drop (H_{max}) for total affected area (A_{total})

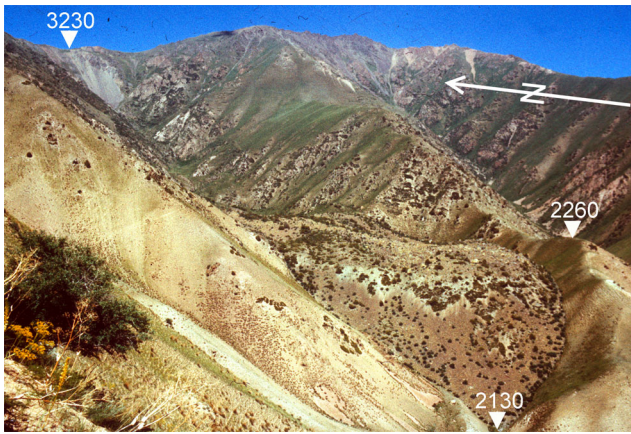| Confinement	Number of cases	Coefficients a	b	c	R-squared	Relative importance V	H_{max}
Frontally confined	294	0.48	0.53	2.52	0.92	0.65	0.35
Laterally confined	68	0.47	0.95	− 0.23	0.94	0.57	0.43
Unconfined	71	0.58	0.49	1.26	0.94	0.65	0.35

Fig. 13 The 3.2-km-long Seit rock avalanche (42.10° N, 74.14° E, Central Tien Shan, Kyrgyzstan, with most of the way lateral and final frontal confinement due to slope bend. After Strom and Abdrakhmatov (2018) with permission from Elsevier

Fig. 14 The 7.4-km-long 1949 Khait rock avalanche (39.19° N, 70.88° E, Southern Tien Shan, Tajikistan) with a 2.6-km-wide distal fan at the flat bottom of the Yarhych River valley. After Strom and Abdrakhmatov (2018) with permission from Elsevier

In contrast, variability of the two-dimensional resultant parameters (A_{total} or A_{dep}) is about one order less than the squared variation of the unidimensional parameter—runout (L). Thus, area increases disproportionally less than the increase of runout, reflecting predominance of forwardly directed motion of debris regardless of confinement conditions, though for the laterally confined and unconfined datasets, it is more pronounced (see Fig. 8). For the laterally confined cases, it is obvious since such confinement prevents transverse debris spreading. However, numerous unconfined rock avalanches have elongated bodies too (see Fig. 1). Thus, question arises—what processes govern the absence of the lateral spreading of debris or, contrarily, its significant spreading in the direction transverse to the initial direction of rock avalanche motion? It can be explained as follows.

Momentum gained by rock avalanche during its initial accelerating descent is a vector value and, thus, can produce motion in the same direction only. So, lateral debris spreading should be caused by additional forces acting in the transverse direction. Transverse forces can be derived from the gravity force affecting the heavily fragmented and rapidly moving rock avalanche body that experience intensive dynamic loading and vibrations. The gravity force causes gradual thinning of moving debris and produces laterally directed force that, in ideal conditions (motion over a flat horizontal surface), is uniform in all directions, both forwarded and transverse.

If such force is high enough to overcome basal friction, debris moves not only straightforward, but laterally as well (it can be seen in Fig. 6 and at the distal part of rock avalanche shown in Fig. 14). Usually, it occurs when rock avalanche moves over a surface composed of material with low shear strength (e.g., flood planes or low terraces with shallow water table, glaciers). If, however, transversely directed force is less than basal shear strength (e.g., at a dry stony alluvial fans) no lateral spreading occurs (Fig. 1) and additional momentum produced by debris thinning just summarizes with the momentum gained from the initial descent, increasing the runout (Strom 2006). To prove (or disprove) this assumption statistically, larger database of unconfined case studies is needed. Such database must also include data on the mechanical properties of the surfaces over which rock avalanches move.
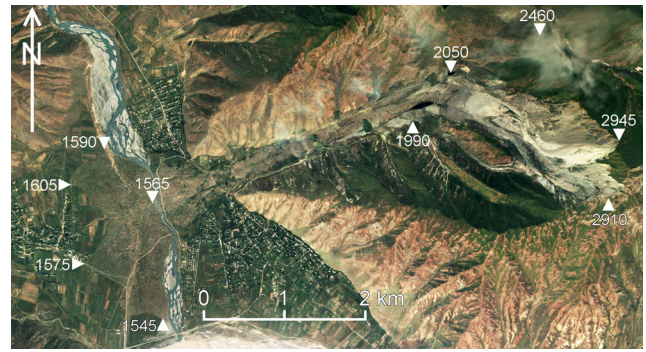
For the frontally confined dataset, the statistical analysis of rock avalanche deposits' shape requires data on the shape of the dammed valleys (U-shape or V-shape) and on the relationships between their depth and width. Compilation of such database and its analysis should be performed in future.

Test and applications

To test the applicability of the newly obtained regressions of $A_{(total; dep)}$ vs. $V \times H_{max}$, we analyzed several unconfined, frontally confined, and laterally confined rock avalanches (rockslides) outside the Central Asia region. Data on their total (A_{total}) and/or deposits' area (A_{dep}) as well as data on volume (V) and height drop (H_{max}) are shown in Table 6. For some of them, different volume and area values have been published. In such cases, we include in the table several variants and consider them as independent case studies. Since the potential energy should be proportional to the source volume, rather than to the resultant deposits' volume, for case studies where source volume was not measured directly, we took it as 80% of the deposits' volume, considering the effects of rockslide debris softening due to increase of the porosity caused by fragmentation, and of the material entrainment. Calculations for different confinement conditions were performed using regression coefficients listed in Table 1.

Area estimates, calculated according to the derived regression equations, differs from the measured values for |32|–|33|% on average (Table 6). Such accuracy can be considered to be acceptable for a simple and fast method that can be used to assess the exposure of elements at risk.

Such approach can be used not only to estimate areas that might be buried by anticipated rock avalanches but also to predict the heights of natural dams that can be formed by large-scale slope failures in frontally confined conditions. It can be exemplified by the blockage that might originate at the suspicious site in the Obi-Khingou River basin (Pamir, Tajikistan), upstream of the Rogun reservoir (Fig. 15) identified on satellite images (Strom and Abdrakhmatov 2018). According to expert's judgment catastrophic collapse of this ~ 1100-m-high slope with anticipated failure volume of about 3×10^8 m³ could create a landslide dam up to 260-m high. Such blockage would

Table 5 Variability of the rock avalanche parameters

Parameter range values	Source parameters				Resultant parameters		
	H_s (km)	H_{max} (km)	H (km)	V (10^6 m^3)	L (km)	A_{dep} (km^2)	A_{total} (km^2)
Min*	0.05	0.05	0.05	0.08	0.19	0.02	0.02
Max	1.84	3.4	3.33	10,000	34	128	144
Max/min ratio	37	68	67	125,000	179	6400	7200

*Rock avalanches usually form when slope failure volume exceeds 1×10^6 m^3. However, several smaller rockslides included in the database also demonstrate flow-like style of motion, thus representing rock avalanches. We also take into account the notice made in Corominas (1996) that "small landslides … display excesses of travel distance similar to large landslides". That is why we did not exclude case studies with volume less than 1 million cubic meters from the analysis

form a dammed lake up to ca. 0.4 km^3 in volume that, in case of its catastrophic breach, could cause quite a disastrous outburst flood (Shakirov et al. 2018). We used both the A_{total} vs. $V \times H_{max}$ and the A_{dep} vs. $V \times H_{max}$ regression equations derived for frontal confinement conditions and got the $A_{total} = 5.57$ km^2 and $A_{dep} = 3.57$ km^2. Considering that the area of the anticipated source zone is about 2 km^2, both approaches provides same estimate of the deposits' area that is used in further analysis.

Shape of the rockslide dam in the V-shaped Ragnou River valley can be modeled, at a first approximation, as a two-pyramid body with triangular base corresponding to the valley cross-section along the dams' crest (Fig. 16). The rhomboid-shape horizontal projection of this body corresponds to the deposits area A_{dep} (~ 3.57 km^2 in our case). Dam height calculated according to a simple geometrical model ($H_{dam} = 3 \times V/A = 3 \times 0.3 / 3.57 \approx 250$ m) is in a good agreement with the previous expert's judgment of ~ 260 m (Shakirov et al. 2018) derived from the time-consuming consecutive adjustment of the assumed headscarp to the manually shaped dam body. Considering standard errors of the regression coefficients, dam height estimates varying from ca. 240 m to ca. 260 m also fit well with the expert's judgment.

These examples demonstrate that the derived relationships can be used successfully to estimate hazard (and associated risks) provided by rock avalanches both directly, in terms of the runout and of the affected area, and indirectly, by assessing parameters of the anticipated rockslide (rock avalanche) dams and subsequent outburst floods.

Discussion—the directions for future research

We must point out that many factors influencing rock avalanche mobility were not considered in our analysis. For example, as we mentioned in the "Dependence of the mobility on the potential energy" section, valleys blocked by frontally confined rock avalanches (rockslides) can have V-shape profile formed by water erosion mainly, or U-shape profile typical of the glacial landforms. It is obvious that the shapes of rock avalanche deposits in such valleys and ratios of their lengths, widths and heights should be different. Most likely, the height of the dam that can be created by rock slope failure of the given volume in the narrow V-shape valley will be larger than that in the U-shape valley with much wider bottom due to larger area of the deposits in the latter case. Resultant shape of rock avalanche deposits might be also influenced by the steepness of the sliding surface, depth of the underground water table at the transition-

deposition zone, style of the along-way debris distribution (Strom 2006), etc.

Besides shape of the transition and deposition zone, obviously influencing the geometry of rock avalanche deposits, it would be interesting to analyze, if rock avalanche mobility depends on the type of the initial slope failure (translational, rotational, wedge slide, etc.; Hungr et al. 2014), and on the lithology of the collapsed rock mass (igneous, sedimentary, metamorphic, terrigenous, carbonate, etc.). However, quantitative and statistically representative assessment of such differences requires a database much larger than the one presented in Strom and Abdrakhmatov (2018) and used in this study. Compilation of larger, likely worldwide database, will allow statistically representative analysis considering more factors than just the confinement.

One more problems that requires additional data collection and analysis – is the relationship between rock avalanche runout and velocity of debris motion. The velocity estimates can be derived from the measurements of the frontal runup or super-elevation along the runout path of the laterally confined case studies (H_{up}). Such analysis, however, requires DEMs with resolution higher than the 3″ SRTM DEM that was used for compiling the database analyzed in this study, since several additional parameters such as steepness and smoothness of the collision zone or of the laterally confining slope should be taken into account. Their correct assessment can be hardly derived from the DEM with 90 m and even 30 m point spacing. Besides, the direct calculation of the velocity based on equalization of the potential and the kinetic energy (velocity = $(2 \times g \times H_{up})^{0.5}$ might be too simplified as it is demonstrated in Pudasaini and Jaboyedov (in press).

Despite the obvious effect of confinement conditions on rock avalanche mobility that has been proven statistically herein, numerous observations of rock avalanche deposits' internal structure, morphology, and grain-size composition show that rock avalanches (rockslides) that moved over terrains with quite different confinement conditions (see, e.g., Heim 1932; Abdrakhmatov and Strom 2006; von Poschinger et al. 2006; Crosta et al. 2015; Dufresne et al. 2016; Reznichenko et al. 2017; Strom and Abdrakhmatov 2018) demonstrate significant similarity of style and extent of debris comminution and of amount of the material entrained in rock avalanche deposits during their motion. It allows assumption that both the dynamic fragmentation (Davies 1982; Davies et al. 2017) and material entrainment are governed by other factors rather than the confinement.

Table 6 Comparison of the measured rock avalanche (rockslide) areas with those calculated according to regression equations A vs. $V \times H_{max}$

Rockslide name, and country	Conf.	Area measured (Am, km²)		H_{max} (km)	Deposits' volume (V_{dep}, km³)	Calculated area (Ac, km²) For measured deposits' volume (V_{dep})	Relative error*	Source volume# (V_s, km³)	Calculated area (Ac, km²) For measured or assumed source volume (V_s)	Relative error*	References
		A_{total}	A_{dep}								
Xinmo	U	1.62		1.25	0.0077	1.29	20	0.0062	1.14	30	Fan et al. 2017
China								0.0051	1.02	37	Ouyang et al. 2017
Yigong	L	9.82		3.1	0.1	6.44	34	0.08	5.7	42	Evans and Delaney 2011
Daguangbao, China	F	7.23		1.5	1.28	13.08	−81	1.024	11.73	−62	Chen et al. 2014
					0.75	10.09	−40	0.6	9.05	−25	Huang et al. 2009, 2012
Vesuvius 5, Italy	U		0.1264	0.636	0.001	0.19	−52	0.0008	0.17	−34	Shaller 1991
Vesuvius 6, Italy	U		0.136	0.36	0.0011	0.15	−8	0.0009	0.13	5	Shaller 1991
Vesuvius 7, Italy	U		0.1456	0.41	0.0012	0.17	−14	0.001	0.15	0	Shaller 1991
Bormio, Itali	F		6	1.62	0.18	3.35	44	0.144	3	50	Heim 1932
Tschirgant, Austria	U?	13.2		1.46	0.16	7.87	40	0.128	6.93	47	Heuberger et al. 1984 and Dufresne et al. 2016
			9.8		0.16	5.81	41	0.128	5.11	48	Dufresne et al. 2016
Köfels, Austria	F	13.5		1.5	3	13.32	1	2.4	11.9	12	Heuberger et al. 1984 and Dufresne et al. 2016
		16			3	19.76	−24	2.4	17.73	−11	
Mt. Granier, France	U	17.5		1.6	0.5	11.81	32	0.4	10.39	41	Eisbacher and Clague 1984
Films, Switzerland	F	40		2.12	12	31.89	20	8	25.99	35	Heim 1932 and von Poschinger et al. 2006
			52		12	31.89	39	8	25.99	50	
		61			12	45.77	25	8	37.6	38	
Baige, China	F	1.62	0.85	0.7				0.0245	0.85	−1	Geological (2018) and Zhang et al. 2019
					Mean (in modulus):		32			33	

*Relative errors are calculated as: (Am-Ac)/Am × 100 (%)

Source volume (if not measured directly) is taken as 80% of the deposits' volume
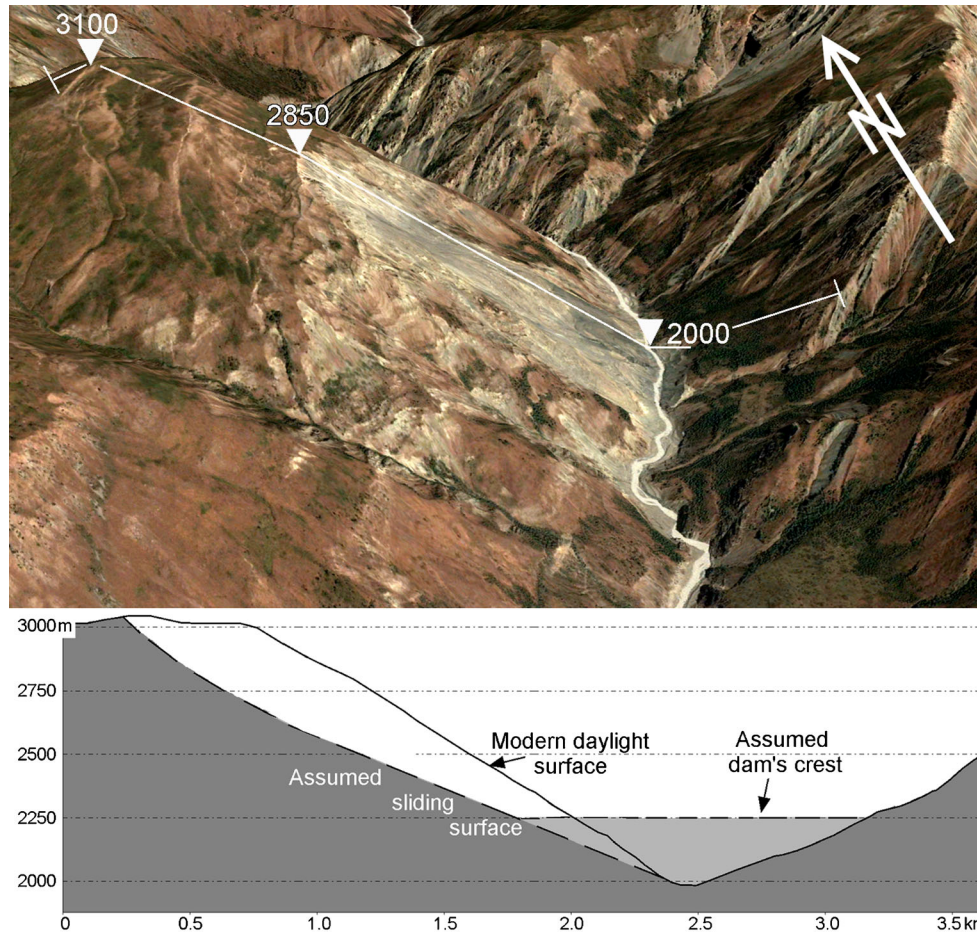
Fig. 15 Evidence of ongoing large-scale slope deformations in the Ragnou River valley (38.92° N, 70.96° E, Northern Pamir, Tajikistan) and the schematic cross-section of the site after anticipated slope failure
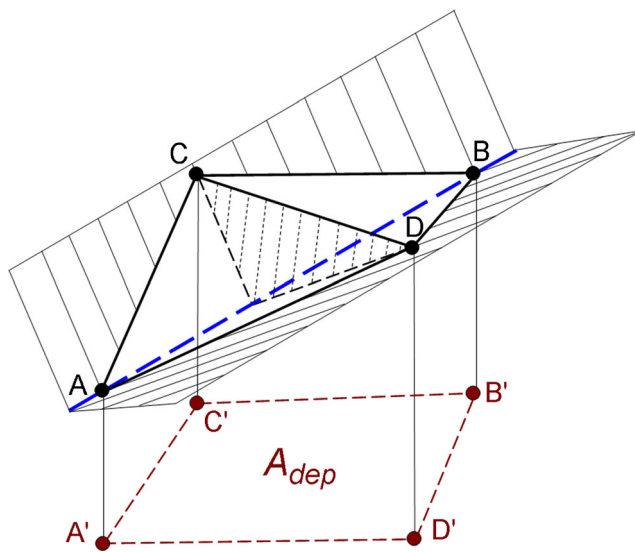

Fig. 16 Schematic geometrical model of a rockslide dam in the V-shaped river valley. A–B, dam length along the stream; C–D, length of the dam crest; A_{dep}, deposits' area

Conclusions

The statistical analysis of a rather large database of the Central Asian bedrock landslides most of which can be classified as rock avalanches, clearly demonstrates that the affected area, either total, or just of the deposits, and their relationships with the $V \times H_{max}$ product provide the optimal characterization of rock avalanche mobility. Best-fit empirical equations of these parameters derived for datasets selected according to the confinement conditions and presented in Table 1 allows most confident prediction of the exposure of elements at risk necessary for rock avalanche hazard and risk assessment. In cases where the rock avalanche runout is the critical parameter, it is optimal to use the relationships between L and $V \times H_{max}$ for the unconfined and frontally confined cases or between L and V regardless of the confinement type, though for the unconfined and frontally confined conditions the previous relationships are preferable due to higher R^2 values (Table 1). The confinement type is an obvious factor that can be described clearly for the past events and anticipated for the potentially hazardous sites, and must be considered in any statistical analysis of the relationships between parameters characterizing rock slope failure source (volume, height drop, or slope height) and parameters characterizing subsequent motion of debris (runout, affected area, etc.).

In future, the statistical analyses considering additional sampling criteria, i.e., more detailed categorization of the confinement, type of the initial slope failure, and climatic and local geological conditions could be performed. It will require, however, compilation of much larger (ideally—worldwide) database.

References

Abdrakhmatov K, Strom A (2006) Dissected rockslide and rock avalanche deposits; Tien Shan Kyrgyzstan. In: Evans SG, Scarascia Mugnozza G, Strom A, Hermanns RL (eds) Landslides from massive rock slope failure. NATO science series: IV: earth and environmental sciences, 49. Springer, New York, pp 551–572

Abele G (1974) Bergstürze in den Alpen, ihre Verbeitung, Morphologie und Folgeerscheinungen, Wissenschaftliche Alpenverein 25, pp 230

Adushkin VV (2006) Mobility of rock avalanches triggered by underground nuclear explosions. In: Evans SG, Scarascia Mugnozza G, Strom A, Hermanns RL (eds) Landslides from massive rock slope failure. NATO science series: IV: earth and environmental sciences. 49. Springer, New York, pp 267–284

Chen Q, Cheng H, Yang Y, Liu G, Liu L (2014) Quantification of mass wasting volume associated with the giant landslide Daguangbao induced by the 2008 Wenchuan earthquake from persistent scatterer InSAR. Remote Sens Environ 152:125–135

Corominas J (1996) The angle of reach as a mobility index for small and large landslides. Can Geotech J 33:260–271

Corominas J, van Westen C, Frattini P, Cascini L, Malet J-P, Fotopoulou S, Catani F, Van Den Eeckhaut M, Mavrouli O, Agliardi F, Pitilakis K, Winter MG, Pastor M, Ferlisi S, Tofani V, Hervás J, Smith JT (2014) Recommendations for the quantitative analysis of landslide risk. Bull Eng Geol Environ 73:209–263

Corominas J, Einstein H, Davis T, Strom A, Zuccaro G, Nadim F, Verdel T (2015) Glossary of terms on landslide hazard and risk. In: Lollino G et al (eds) Engineering geology for society and territory, vol 2. Springer International Publishing, Switzerland, pp 1775–1779

Crosta GB, Imposimato S, Roddeman DG (2003) Numerical modeling of large landslides stability and runout. Nat Hazards Earth Syst Sci 3:523–538

Crosta GB, Frattini P, Valbuzzi E, Hermanns RL (2015) The Cerrillos Negros Giant rock avalanches (Tacna, Peru). In: Lollino G, Giordan D, Crosta GB, Corominas J, Azzam R, Wasowski J, Sciarra N (eds) Engineering geology for society and territory, vol 2. Springer International Publishing, Switzerland, pp 921–924

Davies TR (1982) Spreading of rock avalanche debris by mechanical fluidization. Rock Mech 15:9–24

Davies TR, McSaveney MJ, Reznichenko N (2017) The fate of elastic strain energy in brittle fracture. In: Leith K, Ziegler M, Perras M, Loew S (eds) Progressive rock failure. An ISRM specialized conference, Monte Verità, 5–9 June 2017. ETH, extended abstracts, pp 107–108

Denlinger RP, Iverson RM (2001) Flow of variably fluidized granular masses across three-dimensional terrain: 2. Numerical predictions and experimental tests. J Geophys Res 106B:553–566

Dubovskoi AN, Pernik LM, Strom AL (2008) Experimental simulation of rockslide fragmentation. J Min Sci 44(2):123–130

Dufresne A, Prager C, Bösmeier AS (2016) Insights into rock avalanche emplacement processes by detailed morpho-lithological studies of the Tschirgant deposit (Tyrol Autria). Earth Surf Process Landf 41(5):587–602

Eisbacher GH, Clague JJ (1984) Destructive mass movements in high mountains: hazard and management. Geol Surv Can Pap:84–16

Evans SG, Delaney KB (2011) Characterization of the 2000 Yigong Zangbo River (Tibet) landslide dam and impoundment by remote sensing. In: Evans SG, Hermanns R, Scarascia-Mugnozza G, Strom AL (Eds) Natural and artificial rockslide dams, 133. Lecture Notes in Earth Sciences, pp 543–559

Evans SG, Roberts NJ, Ischuck A, Delaney KB, Morozova GS, Tutubalina O (2009) Landslides triggered by the 1949 Khait earthquake, Tajikistan, and associated loss of life. Eng Geol 109(3–4):195–212

Fan J-R, Zhang X-Y, Su F-H, Ge Y-G, Tarolli P, Yang Z-I, Zeng C, Zeng Z (2017) Geometrical feature analysis and disaster assessment of the Xinmo landslide based on remote sensing data. J Mt Sci 14(9):1677–1688

Geological disaster InSAR technology research center (2018) http://www.vastitude.com.cn/newsinfo/586480.html. (in Chinese)

Grigorian SS (1979) New friction law and mechanism of large-scale rockfalls and landslides, proceedings of Academy of Sciences of USSR, vol 244, pp 846–849 (in Russian)

Griswold JP, Iverson RM (2008) Mobility statistics and automated hazard mapping for debris flows and rock avalanches (ver. 1.1, April 2014): U.S. Geological Survey Scientific Investigations Report 2007–5276, pp 1–59

Heim A (1932) Bergsturz und Menschenleben. Fretz and Wasmuth, Zurich

Heuberger H, Masch L, Preuss E, Schreker A (1984) Quaternary landslides and rock fusion in Central Nepal and the Tyrolen Alps. Mt Res Dev 4:345–362

Hewitt K (1998) Catastrophic landslides and their effects on the upper Indus streams, Karakoram Himalaya, Northern Pakistan. Geomorphology 26:47–80

Howard K (1973) Avalanche mode of motion: implications from lunar examples. Science, New Series 180:1052–1055

Hsü KJ (1975) Catastrophic debris streams (sturzstroms) generated by rock falls. Geol Soc Am Bull 86:129–140

Huang R, Pei X, Zhang W (2009) Further examination on characteristics and formation mechanism of Daguangbao landslide. J Eng Geol 6:725–736

Huang R, Pei X, Fan X, Zhang W, Li S, Li B (2012) The characteristics and failure mechanism of the largest landslide triggered by the Wenchuan earthquake, May 12, 2008. China. Landslides 9:131–142

Hungr O (1995) A model for the runout analysis of rapid flow slides, debris flows, and avalanches. Can Geotech J 32:610–623

Hungr O (2006) Rock avalanche occurrence, process and modelling. In: Evans SG, Scarascia Mugnozza G, Strom A, Hermanns RL (eds) Landslides from massive rock slope failure. NATO science series: IV: earth and environmental sciences, 49. Springer, New York, pp 243–266

Hungr O, McDougall S (2009) Two numerical models for landslide dynamic analysis. Comput Geosci 35:978–992. https://doi.org/10.1016/j.cageo.2007.12.003

Hungr O, Leroueil S, Picarelli L (2014) Varnes classification of landslide types, an update. Landslides 11:167–194

Iverson RM (2006) Forecasting runout of rock and debris avalanches. In: Evans SG, Scarascia Mugnozza G, Strom A, Hermanns RL (eds) Landslides from massive rock slope failure. NATO science series: IV: earth and environmental sciences, 49. Springer, New York, pp 197–209

Iverson RM, Denlinger RP (2001) Flow of variably fluidized granular masses across threedimensional terrain: 1. Coulomb mixture theory. J Geophys Res 106B:537–552

Kilburn CRJ, Sørensen S-A (1998) Runout length of sturzstroms: the control of initial conditions and of fragment dynamics. J Geophys Res 103B:17877–17884

Kobayashi Y (1993) A hypothesis for reduced resistance in large landslides, in Safety and Environmental Issues in Rock Engineering. Proc. of the ISRM Int. Symp. Lisboa, June 21–24, 1993 I. Balkema Rotterdam, pp 335–339

Kobayashi Y (1997) Long runout landslides riding on basal guided wave. In: Marinos K, Tsiambaos S (eds) Engineering geology and the environment. Balkema, Rotterdam, pp 761–766

Legros F (2002) The mobility of long-runout landslides. Eng Geol 63:301–331

Legros F (2006) Landslide mobility and the role of water. In: Evans SG, Scarascia Mugnozza G, Strom A, Hermanns RL (eds) Landslides from massive rock slope failure. NATO science series: IV: earth and environmental sciences, 49. Springer, New York, pp 233–242

Li T (1983) A mathematical model for predicting the extent of a major rockfall. Z Geomorphol 27:473–482

McDougall S, Hungr O (2004) A model for the analysis of rapid landslide motion across three - dimensional terrain. Can Geotech J 41(6):1084–1097. https://doi.org/10.1139/T04-052

Melosh HJ (1986) The physics of very large landslides. Acta Mech 64:89–99

Nadim F, Kjekstad O, Peduzzi P, Herold C, Jaedicke C (2006) Global landslide and avalanche hotspots. Landslides 3:159–173

Nicoletti PG, Sorriso-Valvo M (1991) Geomorphic controls of the shape and mobilily of rock avalanches. Geol Soc Am Bull 103:1365–1373

Ouyang C-J, Zhao W, He S-M, Wang D-P, Zhou S, An H-C, Wang Z-W, Cheng D-X (2017) Numerical modeling and dynamic analysis of the 2017 Xinmo landslide in Maoxian County, China. J Mt Sci 14:1701–1711

Pollet N, Cojean R, Couture R, Schneider J-L, Strom AL, Voirin C, Wassmer P (2005) A slab-on-slab model for the Flims rockslide (Swiss Alps). Can Geotech J 42:587–600

Pudasaini SP, Jaboyedov M (In press) A general analytical model for superelevation. Paper submitted to Landslides

Reznichenko NV, Andrews GR, Geater RE, Strom A (2017) Origin of large hummock deposits ''chukuryi'' in Alai Valley, Northern Pamir: geomorphological and sedimentological investigation. Geomorphology 285:347–362

Sassa K, Fukuoka H, Lee J-H, Shoaei Z, Zhang D, Xie Z et al (1994) Prediction of landslide motion based on the measurement of geotechnical parameters. In: Development of a new cyclic loading ring shear apparatus to study earthquake-induced landslides. Report for Grant-in-Aid for Developmental Scientific Research by the Ministry of Education, Science and Culture, Japan (Project No 03556021), DPRI, Kyoto. pp 72–106

Sassa K, Nagai O, Solidum R, Yamazaki Y, Ohta H (2010) An integrated model simulating the initiation and motion of earthquake and rain induced rapid landslides and its application to the 2006 Leyte landslide. Landslides 7:219–236

Shakirov R, Shilina E, Strom A, Zhirkevich A (2018) Slopes stability in the catchment areas and effect of large-scale rockslide damming on hydraulic projects safety by example of catchment areas of Vakhsh and Siang rivers. Proceedings of 26th ICOLD World Congress. Symposium Hydro Engineering, July 2–3, 2018, Vienna, Austria, pp 2603-2614. https://doi.org/10.3217/978-3-85125-620-8-232

Shaller PJ (1991) Analysis and implications of large Martian and terrestrial landslides, Ph.D. Thesis. California Institute of Technology

Sheidegger AE (1973) On the prediction of the reach and velocity of catastrophic landslides. Rock Mech 5:231–236

Strom AL (2006) Morphology and internal structure of rockslides and rock avalanches: grounds and constraints for their modelling. In: Evans SG, Scarascia Mugnozza G, Strom A, Hermanns RL (eds) Landslides from massive rock slope failure. NATO science series: IV: earth and environmental sciences 49, pp 305–328

Strom A (2018) Large-scale rockslide inventory of the Central Asia region: data and analysis. In: Shakoor A and Cato K (eds) IAEG/AEG annual meeting proceedings, San Francisco, California, 2018, 1 pp 145–153. https://doi.org/10.1007/978-3-319-93124-I_18

Strom A, Abdrakhmatov K (2018) Rockslides and rock avalanches of Central Asia: distribution, morphology, and internal structure. Elsevier. ISBN: 978-0-12-803204-6

Strom A, Pernik L (2013) Modeling of debris crushing during rock avalanche motion. Geophys Res Abst 15, EGU2013 p 1373

von Poschinger A, Wassmer P, Maisch M (2006) The Flims rockslide: history of interpretation and new insights. In: Evans SG, Scarascia Mugnozza G, Strom A, Hermanns RL (eds) Landslides from massive rock slope failure. NATO science series: IV: earth and environmental sciences, vol 49. Springer, Heidelberg, pp 329–356

Zhang Z, He S, Liu W, Liang H, Yan S, Deng Y, Bai X, Chen Z (2019) Source characteristics and dynamics of the October 2018 Baige landslide revealed by broadband seismograms. Landslides 16:777–785. https://doi.org/10.1007/s10346-019-01145-3

A. Strom (✉)
Geodynamics Research Center Ltd.,
Moscow, Russia
Email: strom.alexandr@yandex.ru

A. Strom · H. Lan
School of Geological Engineering and Geomatics,
Chang'an University,
Xi'an, China

L. Li · H. Lan
State Key Laboratory of Resources and Environmental Information System, Institute of Geographic Sciences and Natural Resources Research,
Chinese Academy of Sciences,
Beijing, China